Title

Electrochemical CO2 Reduction over Compressively Strained CuAg Surface Alloys with Enhanced Multi-Carbon Oxygenate Selectivity

Journal

Journal of the American Chemical Society, 139(44)

ISSN

0002-7863

Authors

Clark, Ezra L
Hahn, Christopher
Jaramillo, Thomas F
et al.

Publication Date

2017-11-08

DOI

10.1021/jacs.7b08607

Peer reviewed

JACS
JOURNAL OF THE AMERICAN CHEMICAL SOCIETY
Article
Cite This: J. Am. Chem. Soc. 2017, 139, 15848-15857
pubs.acs.org/JACS

Electrochemical CO_2 Reduction over Compressively Strained CuAg Surface Alloys with Enhanced Multi-Carbon Oxygenate Selectivity

Ezra L. Clark,[†,‡] Christopher Hahn,[§,∥] Thomas F. Jaramillo,[§,∥] and Alexis T. Bell*[,†,‡]

[†]Joint Center for Artificial Photosynthesis, Lawrence Berkeley National Laboratory, Berkeley, California 94720, United States
[‡]Department of Chemical and Biomolecular Engineering, University of California, Berkeley, California 94720, United States
[§]SUNCAT Center for Interface Science and Catalysis, SLAC National Accelerator Laboratory, Menlo Park, California 94025, United States
[∥]Department of Chemical Engineering, Stanford University, Stanford, California 94305, United States

Supporting Information

ABSTRACT: The electrochemical reduction of carbon dioxide using renewably generated electricity offers a potential means for producing fuels and chemicals in a sustainable manner. To date, copper has been found to be the most effective catalyst for electrochemically reducing carbon dioxide to products such as methane, ethene, and ethanol. Unfortunately, the current efficiency of the process is limited by competition with the relatively facile hydrogen evolution reaction. Since multi-carbon products are more valuable precursors to chemicals and fuels than methane, there is considerable interest in modifying copper to enhance the multi-carbon product selectivity. Here, we report our investigations of electrochemical carbon dioxide reduction over CuAg bimetallic electrodes and surface alloys, which we find to be more selective for the formation of multi-carbon products than pure copper. This selectivity enhancement is a result of the selective suppression of hydrogen evolution, which occurs due to compressive strain induced by the formation of a CuAg surface alloy. Furthermore, we report that these bimetallic electrocatalysts exhibit an unusually high selectivity for the formation of multi-carbon carbonyl-containing products, which we hypothesize to be the consequence of a reduced coverage of adsorbed hydrogen and the reduced oxophilicity of the compressively strained copper. Thus, we show that promoting copper surface with small amounts of Ag is a promising means for improving the multi-carbon oxygenated product selectivity of copper during electrochemical CO_2 reduction.

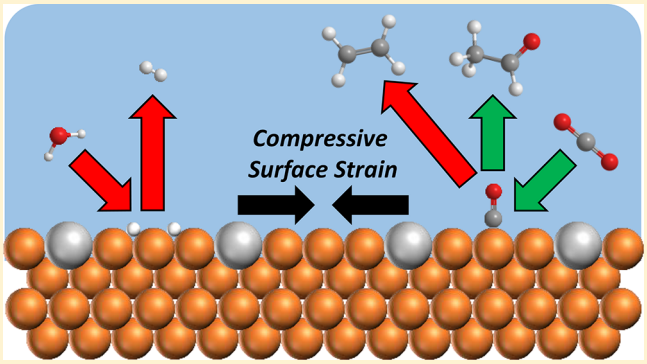

INTRODUCTION

Atmospheric carbon dioxide is a potential source of renewable carbon for the production of fuels and chemicals. For this process to be sustainable, the hydrogen required for CO_2 reduction must be derived from water and the necessary energy must be supplied by a renewable source, such as solar radiation. One approach to this goal is the utilization of electrical energy generated by photovoltaics to drive the electrochemical CO_2 reduction reaction (CO_2RR).[1−3] Previous research has shown that the overall rate of the CO_2RR and the distribution of products formed depend primarily on the electrocatalyst used as the cathode. Copper is the only monometallic electrocatalyst capable of reducing CO_2 into potential fuels or multi-carbon chemicals with a total Faradaic efficiency (FE) in excess of 1%.[4,5] Experimental and theoretical studies have demonstrated that carbon monoxide reduction is the overpotential-determining step in the reduction of CO_2 to hydrocarbons and alcohols over Cu.[6−11] The principal products formed by the reduction of CO are methane (CH_4), ethene (C_2H_4), and ethanol (C_2H_5OH).[7,12] However, a variety of other multi-carbon alcohols, aldehydes, and carboxylic acids are also produced, albeit in trace quantities.[7,12] Since multi-carbon products are more valuable precursors to chemicals and fuels than CH_4, there is considerable interest in modifying Cu to enhance the multi-carbon product selectivity (see Supporting Information, SI-1). Unfortunately, the FE of multi-carbon product generation over Cu is limited by parasitic loss of total current density to the relatively facile hydrogen evolution reaction (HER). Thus, recent studies have focused on suppressing HER and enhancing the multi-carbon product selectivity. These studies have revealed that the applied potential,[7,12,13] surface morphology,[14−18] cation identity,[19−21] and buffer concentration[22−24] influence the product distribution obtained over Cu. While alloying is another means for tuning the product distribution,[25] no multi-metallic electrocatalyst has been discovered with a multi-carbon product selectivity superior to pure Cu.[26−29] In fact, it has been shown

Received: August 13, 2017
Published: October 7, 2017

DOI: 10.1021/jacs.7b08607
J. Am. Chem. Soc. 2017, 139, 15848−15857

that the multi-carbon product selectivity observed over Cu-based alloys decreases systematically with the Cu content, suggesting that neighboring Cu atom ensembles are required for efficient C−C coupling.[29]

Under the conditions of CO_2RR a substantial portion of the Cu surface is covered by adsorbed CO, which suppresses HER by both reducing the effective number of electrocatalytically active surface sites and by weakening the H adsorption energy of the remaining open sites.[7,30−32] As a result, the surface coverage of CO influences the rate of HER as well as the distribution of products derived from CO, with higher CO coverages presumably inhibiting HER and enhancing the multi-carbon product selectivity. Consistent with this interpretation, the ratio of CH_4 to C_2H_4 has been observed to scale directly with the FE for H_2.[22,33,34] At potentials cathodic of −1 V vs RHE the FEs for H_2 and CH_4 increase rapidly at the expense of C_{2+} products over Cu.[12] The onset potential of this selectivity shift corresponds to the potential at which Cu reduces nearly all of the CO that it produces into hydrocarbons or alcohols (see Supporting Information, SI-2), suggesting that this selectivity shift is caused by a reduced coverage of adsorbed CO. Thus, we hypothesized that supplying additional CO to Cu by co-locating domains of Cu with those of a CO-generating metal would enhance the C_{2+} product selectivity because the elevated CO concentration in the vicinity of the cathode will result in a higher steady-state coverage adsorbed on Cu (see Supporting Information, SI-3).[35] To this end, we identified the Cu−Ag system as the optimal bimetallic system to probe this hypothesis because Ag produces more CO than Cu at a given potential and because Cu and Ag are virtually immiscible in the bulk at all compositions at room temperature (see Supporting Information, SI-4).[36,37]

In the balance of this paper, we report the results of our investigation of CO_2RR over CuAg bimetallic electrodes and surface alloys. While we have observed evidence of synergy between Cu and Ag, the data do not support our original hypothesis that this is a result of CO spillover. Instead, we have discovered that Ag promotes the Cu surface by the formation of a CuAg surface alloy that induces compressive strain in the Cu surface atoms. The compressive strain in the Cu surface results in an observable shift of the valence band structure of Cu to deeper levels. This modification weakens the adsorption energy of H, resulting in a 60−75% reduction in the HER activity of Cu during CO_2RR. Interestingly, the inhibition of HER does not impact the ability of Cu to produce products derived from CO, leading to a 10−15% boost in the total FE for C_{2+} products. Furthermore, the distribution of products derived from CO changes in favor of multi-carbon carbonyl-containing products at the expense of hydrocarbons. This product selectivity modification is attributed to reduced rates of C−O bond scission resulting from the suppression of HER and the reduced oxophilicity of the compressively strained Cu, which presumably inhibits the ability of Cu to reduce these carbonyl-containing intermediate products further.

EXPERIMENTAL SECTION

Electrode Preparation. All CuAg bimetallic electrodes were prepared by melting physical mixtures of Cu (99.999%) and Ag (99.999%) in the desired atomic ratios under Ar in a vacuum arc furnace. The molten mixtures were rapidly quenched in deionized (DI) water and cold-rolled into foils. The bimetallic foils were then polished with a series of sandpapers (600, 1200, and 2500 grit 3M) and sonicated in DI water for 30 min before any characterization or electrochemical testing was performed.

Cu(100) thin films were prepared using an AJA ATC Orion-5 magnetron sputtering system. Polished Si(100) wafers (1−10 Ω·cm Virginia Semiconductor) were utilized as substrates and were etched immediately before deposition using 10 wt% HF.[38,39] Cu (99.999% Kurt J. Lesker) was then sputtered onto the etched wafers at a rate of 1 Å/s to a thickness of 100 nm under Ar. The Cu films were then exposed to a deaerated solution of $AgNO_3$ at 50 °C for 5 min in order to galvanically exchange Ag into the Cu surface. The surface Ag content was controlled by adjusting the $AgNO_3$ concentration in the galvanic exchange solution.

Electrode Characterization. The crystal structure of the bimetallic electrodes and epitaxial Cu films was analyzed with a Rigaku Smartlab X-ray diffractometer (XRD) using Cu Kα radiation (40 kV, 40 mA). The diffractometer was equipped with parallel beam optics and a 0.5° parallel slit analyzer in order to mitigate measurement errors arising from the surface curvature of the bimetallic foils. The bulk crystal structure was analyzed by conducting symmetric measurements while the near-surface crystal structure was analyzed by conducting asymmetric measurements with the incident radiation beam fixed at a grazing angle of 0.5°. The compositions of the observed phases were calculated using Vegard's law and their average crystallite sizes were calculated using the Scherrer equation. The orientation of the Cu crystallites with respect to the Si substrate were determined by conducting symmetric in-plane φ scans at the Bragg reflections corresponding to both Si(111) and Cu(111). The degree of preferred orientation in the epitaxial Cu thin films was determined by conducting symmetric out-of-plane Ω scans, or rocking curves, at the Bragg condition corresponding to Cu(200).

The bulk composition of the bimetallic electrodes was measured using an FEI Quanta FEG 250 scanning electron microscope (SEM) equipped with a Bruker Quantax energy dispersive spectrometer (EDS). Elemental quantification was conducted by measuring the X-ray emission from the Cu K and the Ag L levels upon excitation by an electron beam (15 kV). Each electrode was analyzed at 10 distinct positions in order to assess the spatial uniformity of the measured bulk composition. The standard deviation of the measured bulk composition was found to be <1 at.% for all bimetallic electrodes, indicating that they are compositionally uniform at the micrometer length scale.

The near-surface composition and valence band structure of the bimetallic electrodes and surface alloys were measured using a Kratos Axis Ultra DLD X-ray photoelectron spectrometer (XPS). All spectra were acquired using monochromatized Al Kα radiation (15 kV, 15 mA). Ar sputtering of the sample surface was avoided in order to prevent surface composition changes resulting from the nonequivalent sputtering rates of Cu and Ag unless explicitly stated otherwise. Where applicable, Ar sputtering of the sample surface was conducted using a focused Ar ion beam (5 kV). The kinetic energy scale of the measured core level spectra was calibrated by setting the C 1s binding energy to 284.8 eV. Elemental quantification was conducted by measuring the photoelectron emission from the Cu 2p and Ag 3d orbitals using a Shirley background and normalizing their integrated areas by an internally calibrated relative sensitivity factor. The Cu 2p spectral features were fit to three individual components (Cu^0, Cu^+, and Cu^{2+}) using the CasaXPS software. The kinetic energy scale of the measured valence band spectra was calibrated by setting the maximum rate of signal loss to 0 eV. Angle-resolved XPS (ARXPS) was conducted by measuring photoelectrons ejected at an angle of 30° from the sample surface, which results in twice the surface sensitivity compared to photoelectrons collected normal to the sample surface. The surface composition of the bimetallic electrodes and surface alloys were measured by ion scattering spectroscopy (ISS) using the same instrument. All ISS spectra were acquired using a focused He ion beam (1 kV). Elemental quantification was conducted by integrating the Cu and Ag spectral features using a linear background and normalizing their integrated areas by an internally calibrated relative sensitivity factor.

DOI: 10.1021/jacs.7b08607
J. Am. Chem. Soc. 2017, 139, 15848−15857

Electrochemical Characterization. All electrochemical measurements were conducted in a custom gastight electrochemical cell machined from PEEK.[40] The cell was sonicated in 20 wt% nitric acid and thoroughly rinsed with DI water prior to all experimentation. The working and counter electrodes were parallel and separated by an anion-conducting membrane (Selemion AMV AGC Inc.). Gas dispersion frits were incorporated into both electrode chambers in order to provide ample electrolyte mixing. The exposed geometric surface area of each electrode was 1 cm^2 and the electrolyte volume of each electrode chamber was 1.8 mL. The counter electrode was a glassy carbon plate (Type 2 Alfa Aesar) that was also sonicated in 20 wt% nitric acid prior to all experimentation. Platinum was not used as the anode due to the possibility of contaminating the cathode.[41] The working electrode potential was referenced against a Ag/AgCl electrode (Innovative Instruments Inc.) that was calibrated against a homemade standard hydrogen electrode. A 0.05 M Cs_2CO_3 (99.995% Sigma-Aldrich) solution prepared using 18.2 MΩ DI water was used as the electrolyte. This electrolyte was selected because it has been shown to enhance the C_{2+} product selectivity obtained over polycrystalline Cu.[19−21] Metallic impurities in the as-prepared electrolyte were removed before electrolysis by chelating the solution with Chelex 100 (Na form Sigma-Aldrich).[42] Both electrode chambers were sparged with CO_2 (99.999% Praxair Inc.) at a rate of 5 sccm for 30 min prior to and throughout the duration of all electrochemical measurements. Upon saturation with CO_2 the pH of the electrolyte was 6.8, which was maintained throughout the duration of chronoamperometry.

Electrochemistry was performed using a Biologic VSP-300 potentiostat. All electrochemical measurements were recorded versus the reference electrode and converted to the RHE scale. Potentiostatic electrochemical impedance spectroscopy (PEIS) was used to determine the uncompensated resistance (R_u) of the electrochemical cell by applying voltage waveforms about the open-circuit potential with an amplitude of 20 mV and frequencies ranging from 50 Hz to 500 kHz (see Supporting Information, SI-5). The potentiostat compensated for 85% of R_u *in situ* and the last 15% was postcorrected to arrive at accurate potentials. The redox properties of the bimetallic electrodes were assessed by performing cycling voltammetry from −0.3 to +1.1 V vs RHE at a scan rate of 10 mV/s until a stable voltammogram was obtained, which occurred in less than 10 cycles. The electrocatalytic activity of each bimetallic electrode and surface alloy was assessed by conducting chronoamperometry at −1.05 and −1.00 V vs RHE, respectively, for 70 min. Each electrode was tested at least three times in order to ensure the statistical relevance of the observed trends.

Product Analysis. The effluent from the electrochemical cell was introduced directly into the sampling loop of an Agilent 7890B gas chromatograph (GC) equipped with a pulsed-discharge helium ionization detector (PDHID). The effluent was sampled after the first 10 min of chronoamperometry and every 14 min thereafter. The constituents of the gaseous sample were separated in He (99.9999% Praxair Inc.) using a Hayesep-Q capillary column (Agilent) in series with a packed ShinCarbon ST column (Restek Co.). After sampling the reaction effluent the column oven was maintained at 50 °C for 1 min followed by a temperature ramp at 30 °C/min to 250 °C, which was maintained for the duration of the analysis. The signal response of the PDHID was calibrated by analyzing a series of NIST-traceable standard gas mixtures (Airgas Inc.) (see Supporting Information, SI-6).

The electrolyte from both electrode chambers was collected after electrolysis and analyzed using a Thermo Scientific UltiMate 3000 liquid chromatograph (HPLC) equipped with a refractive index detector (RID). The electrolyte samples were stored in a refrigerated autosampler until analyzed in order to minimize the evaporation of volatile liquid-phase reaction products. The liquid-phase products contained in a 10 μL aliquot were separated using a series of two Aminex HPX 87-H columns (Bio-Rad Inc.) and a 1 mM sulfuric acid eluent (99.999% Sigma-Aldrich). The column oven was maintained at 60 °C for the duration of the analysis. The signal response of the RID was calibrated by analyzing standard solutions of each product at a concentration of 1, 10, and 50 mM (see Supporting Information, SI-7).

RESULTS AND DISCUSSION

Characterization of the As-Prepared Bimetallic Electrodes. XRD and GIXRD measurements were carried out to determine the bulk and near-surface crystal structures, respectively, of the bimetallic electrodes (see Supporting Information, SI-8 and SI-9). Figure 1 shows the asymmetric

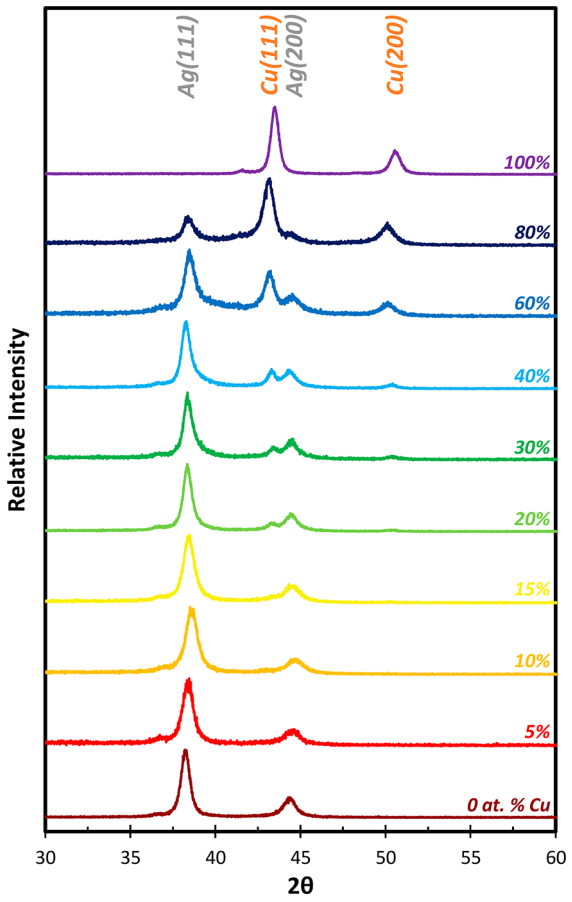

Figure 1. Asymmetric GIXRD patterns of the CuAg bimetallic electrodes.

GIXRD patterns of the bimetallic electrodes. The presence of diffraction peaks associated with Cu and Ag and the absence of any diffraction peaks associated with a CuAg alloy phase confirms the phase-segregated nature of the electrodes. Furthermore, the minimal shift of the Cu and Ag diffraction peak positions indicates that the Cu and Ag phases have undergone minimal alloying (<3 at.% on average as calculated by Vegard's law). The near-surface Cu and Ag crystallites were calculated to be 10−15 nm in size and were observed to be preferentially oriented in the (111) direction, despite that GIXRD does not probe lattice planes parallel to the electrode surface. Moreover, the relative intensities of the Cu and Ag diffraction peaks in the near-surface region were found to be independent of the bulk composition (see Supporting Information, SI-10).

The bulk compositions of the as-prepared bimetallic electrodes were quantified by EDS (see Supporting Information, SI-11), the near-surface compositions were quantified by XPS (see Supporting Information, SI-12), and the surface

DOI: 10.1021/jacs.7b08607
J. Am. Chem. Soc. 2017, 139, 15848−15857

compositions were quantified by ISS (see Supporting Information, SI-13). Both XPS and ISS yielded results that were completely consistent with EDS, as shown in Figure 2A. Thus, the average composition of the as-prepared bimetallic electrodes was determined to be independent of depth from the surface.

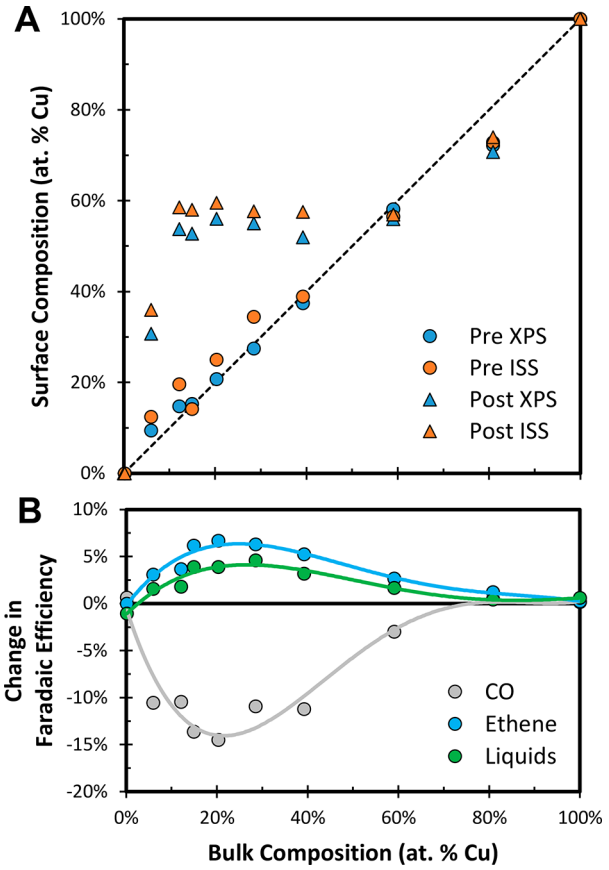

Figure 2. (A) Near-surface (XPS) and surface (ISS) compositions of the CuAg bimetallic electrodes before and after CO_2RR. (B) Transient changes in the reaction selectivity observed over the CuAg bimetallic electrodes during the first 20 min of electrolysis at −1.05 V vs RHE.

Transient Reaction Selectivity of the Bimetallic Electrodes. The FEs of the gaseous products produced over the CuAg bimetallic electrodes were monitored with time during CO_2RR in order to determine the stability of the electrodes. While the FEs of the gaseous products were constant over pure Cu and Ag, all of the bimetallic electrodes exhibited changes in the product distribution over the first 20 min of electrolysis. These changes were most significant for the Ag-rich bimetallic electrodes and were characterized by a drop in the FE of CO and an increase in the total FE of products derived from CO, as shown in Figure 2B. These observations suggest that the surface of the bimetallic electrodes undergo Cu enrichment during this transient period. To confirm this hypothesis the near-surface and surface compositions of the bimetallic electrodes were measured by XPS and ISS after chronoamperometry. As shown in Figure 2A, the XPS and ISS measurements taken after chronoamperometry confirm that Cu surface enrichment occurs over the course of electrolysis. Furthermore, the magnitude of the reaction selectivity changes over the transient period scale with the magnitude of the observed Cu surface enrichment, confirming that the transient reaction selectivity is caused by the segregation of Cu to the electrode surface (see Supporting Information, SI-14). However, no change in the average crystallite size or extent of alloying was observed by GIXRD after electrolysis, potentially due the inadequate surface sensitivity of the measurement. Interestingly, the Ag-rich bimetallic electrodes undergo more Cu surface enrichment than those that are Cu-rich. This suggests that Cu initially dissolved in the Ag phase segregates to the surface, since the fraction of Cu present in the bimetallic electrodes that is dissolved in the Ag phase increases with the bulk Ag content. The consistency of the measured near-surface and surface compositions suggests that the segregation of Cu to the surface of the Ag phase forms a Cu-rich skin with a thickness ≥1 nm. The driving force for the segregation of Cu to the surface of the Ag phase is hypothesized to be the stronger interaction of CO with Cu than Ag.[9,10]

Steady-State Selectivity of the Bimetallic Electrodes. The steady-state CO_2 consumption rate observed over all of the bimetallic electrodes was lower than the diffusion limited consumption rate observed over polycrystalline Ag, ensuring that the trends reported herein are not excessively affected by mass transfer effects (see Supporting Information, SI-15). Since the bimetallic electrodes with bulk compositions of 10−60 at.% Cu enrich to roughly the same surface composition at steady state, the results obtained over all of these electrocatalysts were averaged together. The H_2 FE observed over the bimetallic electrodes was significantly lower than that observed over polycrystalline Cu, with the nominal bimetallic electrodes exhibiting H_2 FEs ∼ 30% lower than observed over pure Cu (see Supporting Information, SI-16). A large fraction of this current is instead utilized to produce CO, which is produced with an average FE of ∼20% over the nominal bimetallic electrodes. However, a portion of this current is also utilized to produce products derived from CO, with a total FE ∼10% higher observed over the nominal bimetallic electrodes than pure Cu. Interestingly, the bimetallic electrodes are also unusually selective for the formation of multi-carbon oxygenates, producing a maximum FE of ∼35%, which is more than double the total oxygenate FE observed over pure Cu. Acetate and acetaldehyde account for a substantial portion of the multi-carbon oxygenate selectivity, reaching a combined FE of ∼15%, which is significant because neither of these products is produced over pure Cu with a FE above 1%.

Steady-State Activity of the Bimetallic Electrodes. The steady-state partial current densities of the major reaction products are plotted as a function of the steady-state near-surface composition of the CuAg bimetallic electrodes in Figure 3. The steady-state activity of the bimetallic electrodes did not display any dependence on the extent of alloying observed in the individual phases by XRD or GIXRD. However, it is apparent that the HER activity is suppressed compared to what would be expected if the bimetallic electrodes behaved as a linear combination of Cu and Ag, with the nominal bimetallic electrodes producing ∼75% less H_2 than pure Cu. Conversely, the total partial current density to products derived from CO scales linearly with the surface Cu content, meaning that the suppression of HER does not inhibit the ability of Cu to produce products derived from CO. Thus, the enhanced selectivity to multi-carbon products observed over the bimetallic electrodes is a consequence of the suppression of HER and not the enhancement of CO_2RR. The suppression of HER could be explained in terms of an enhanced coverage of CO adsorbed on Cu due to spillover from Ag. However, if

DOI: 10.1021/jacs.7b08607
J. Am. Chem. Soc. 2017, 139, 15848−15857

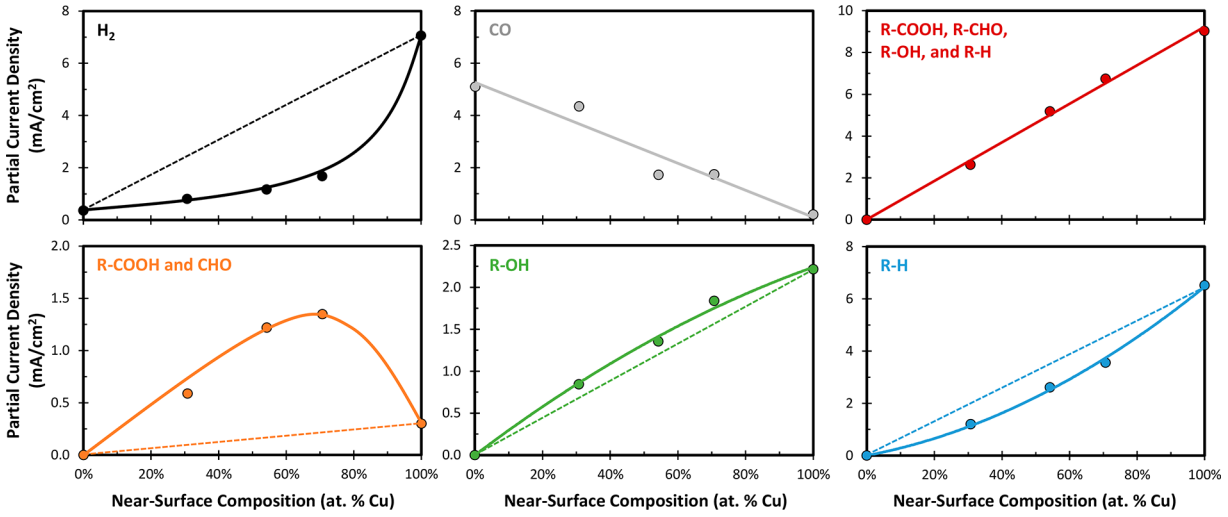

Figure 3. Steady-state partial current densities observed over the CuAg bimetallic electrodes at an applied potential of −1.05 V vs RHE as a function of the steady-state near-surface composition, as quantified by XPS after electrolysis. The solid line is meant to guide the eye while the dotted line displays what was expected to be observed had the CuAg bimetallic electrodes behaved as a linear combination of Cu and Ag.

significant CO spillover occurred, the observed CO partial current density would be lower than expected for a linear combination of Cu and Ag. Conversely, the CO generation rate scales linearly with the surface Ag content of the bimetallic electrodes. Therefore, the absence of missing CO does not support our initial hypothesis that CO generated over Ag is consumed over Cu. As mentioned previously, the distribution of products derived from CO is modified compared to what is typically observed over pure Cu, with a ∼400% enhancement of the generation rate of multi-carbon carbonyl-containing products compared to pure Cu. This activity boost is accompanied by a concomitant suppression of the hydrocarbon partial current density, which is predominately ethene. Additional experiments conducted over a Ag mesh backed by a Cu foil confirmed that an elevated local CO concentration does not significantly impact the distribution of products obtained over Cu, confirming that CO spillover is not the cause of the modified product distribution observed over the bimetallic electrodes (see Supporting Information, SI-17).

The total partial current densities to products produced over Cu were normalized by the steady-state near-surface Cu content and plotted as a function of the steady-state near-surface composition in order to gain insight into the dependence of the activity of the Cu phase in the bimetallic electrodes on the near-surface composition. As shown in Figure 4, the addition of Ag into Cu suppresses the HER activity of the Cu phase by ∼75% during CO_2RR. Conversely, the addition of Ag into Cu does not impact the total partial current density to products derived from CO, as previously stated. However, the distribution of products derived from CO does change, with the generation rate of carbonyl-containing products being enhanced at the expense of hydrocarbons. Interestingly, the activity of the Cu phase in the bimetallic electrodes is independent of the near-surface composition, suggesting that Ag may act as a surface promoter of Cu. However, this promoter effect saturates before a bulk Ag phase forms, which is why the Cu phase is identical in electrocatalytic activity in all the bimetallic electrodes studied here. Thus, the Cu phase in the bimetallic electrodes is expected to have a surface atomic arrangement that is independent of the near-surface composition. In the next section, we explore the possibility that small

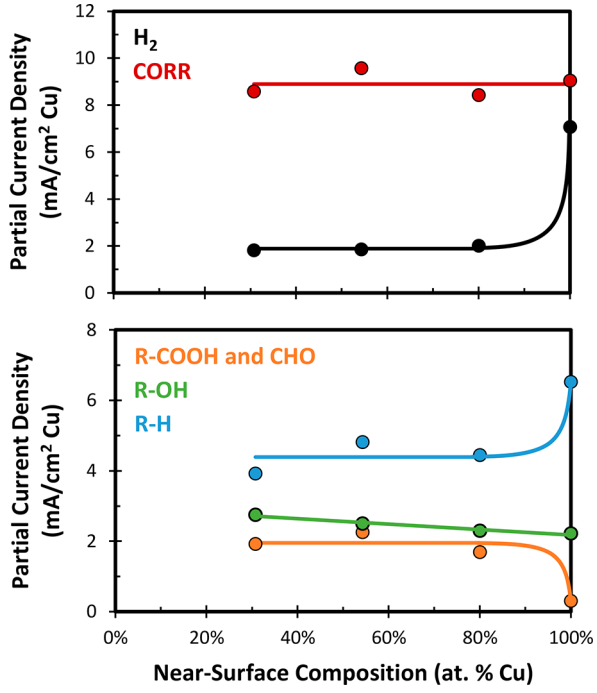

Figure 4. Steady-state activity of the Cu phase in the bimetallic electrodes at an applied potential of −1.05 V vs RHE as a function of the steady-state near-surface Cu content.

amounts of Ag can promote the Cu surface and shift the product distribution to favor multi-carbon oxygenates at the expense of H_2 and hydrocarbons.

Cu(100)+Ag Surface Alloys. Epitaxial Cu(100) thin films have been observed to exhibit surface adlattices upon electrochemical reduction that are identical to their bulk structure,[43] which makes them a well-defined foundation for a systematic study of the effect of Ag surface promotion on the electrocatalytic activity of Cu. Accordingly, Cu(100)+Ag electrodes were prepared by epitaxial growth of Cu on Si(100) followed by galvanic exchange with Ag. As shown in Figure 5A, Cu(111) X-ray pole figures of the Cu(100) thin films exhibit the 4-fold symmetry characteristic of Cu(100),

DOI: 10.1021/jacs.7b08607
J. Am. Chem. Soc. 2017, 139, 15848−15857

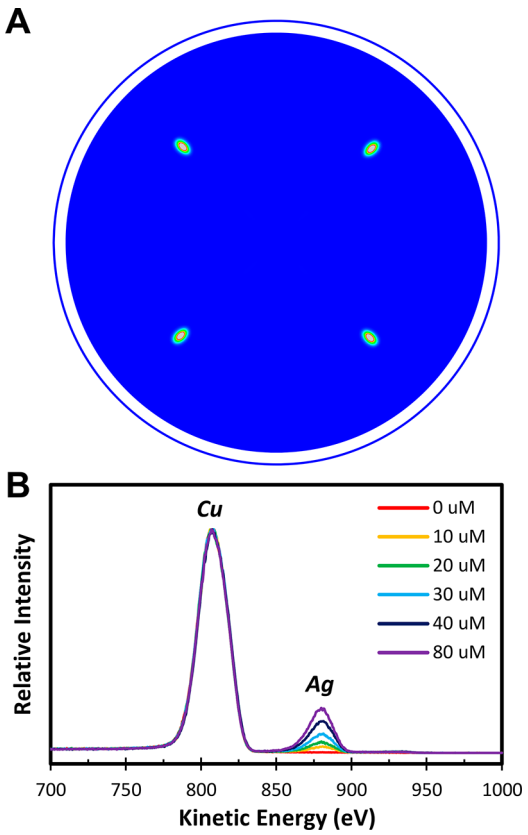

Figure 5. (A) Cu(111) X-ray pole figure of the epitaxial Cu(100) thin film deposited on Si(100). (B) ISS spectra of the Cu(100)+Ag electrodes.

confirming the epitaxial nature of the Cu thin films (see Supporting Information, SI-18). The Ag loading on the Cu(100) thin films was quantified by XPS after galvanic exchange and was found to scale with the concentration of $AgNO_3$ in the galvanic exchange solution (see Supporting Information, SI-19). As shown in Figure 5B, ISS confirmed that the Ag was incorporated into the Cu(100) surface. The direct correlation between the integrated area of the Ag ISS peak with the near-surface Ag composition, as quantified by XPS, suggests that all of the exchanged Ag atoms are located at the electrode surface (see Supporting Information, SI-20).

The electrocatalytic activity of the Cu(100)+Ag electrodes were measured under conditions similar to those utilized to assess the CuAg bimetallic electrodes. Unlike the bimetallic electrodes, the Cu(100)+Ag electrodes did not display significant changes in reaction selectivity with time, suggesting that the surface structure and composition are stable throughout the duration of electrolysis (see Supporting Information, SI-21). This stability is expected because the immiscibility of Cu and Ag prevents Ag from diffusing into the bulk of the Cu thin film during electrolysis. As the near-surface Ag content of the Cu(100)+Ag electrodes increased, the steady-state activity more closely resembled that observed over the Cu phase in the bimetallic electrodes, as shown in Figure 6. In fact, the HER activity of the Cu(100) thin films decreased by ~60% by the incorporation of ~3 at.% Ag into the near-surface region. Furthermore, the suppression of HER had a negligible impact on the ability of Cu to reduce CO, resulting in a 10% boost in the multi-carbon product FE compared to pure Cu(100). Furthermore, the addition of Ag into the Cu(100)

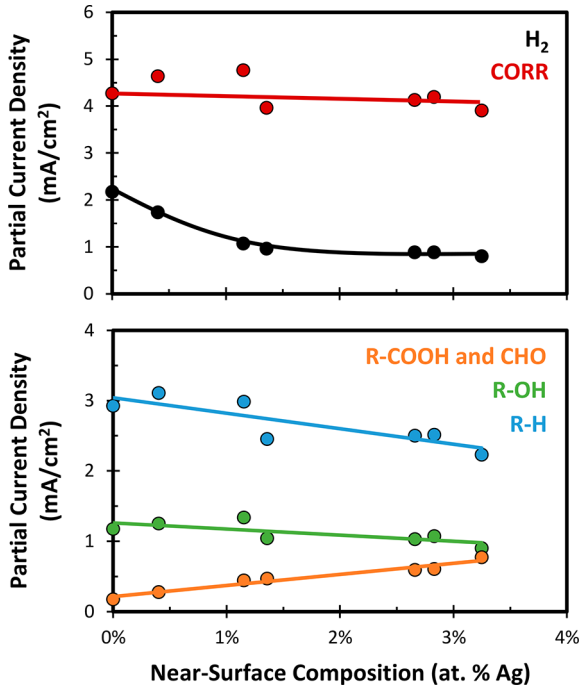

Figure 6. Steady-state activity of the Cu(100)+Ag electrodes at an applied potential of −1 V vs RHE as a function of the near-surface composition, as measured by XPS.

surface enhanced the rate of carbonyl-containing product generation at the expense of ethene. Thus, the activity trends observed over the Cu phase in the bimetallic electrodes were qualitatively reproduced by adding <3 at.% Ag into the near-surface region of Cu(100), confirming the role of Ag as a surface promoter of Cu.

Electronic Modifications of Cu Induced by Compressive Strain. While Cu and Ag are completely immiscible in the bulk at room temperature,[37] surface science studies have revealed that they exhibit limited surface miscibility.[44] In fact, the addition of Ag adatoms onto Cu(100) single crystals was found to spontaneously result in the formation of a random substitutional surface alloy at room temperature with a maximum Ag content of ~16 at.% in the top layer of atoms.[44] Since the penetration depth of XPS is ~10 atomic layers, a Ag-saturated Cu(100)+Ag surface alloy would have a near-surface composition of ~1.6 at.% Ag, which we have found to be the optimal near-surface composition for the suppression of HER. Interestingly, surface scientists have observed that the Ag atoms incorporated into the Cu(100) surface have fewer Ag nearest neighbors than would be expected for an ideal solution. This occurs because the substitution of larger Ag atoms into the Cu surface induces compressive strain in the surrounding Cu atoms, which causes the incorporated Ag atoms to repel one another.[44,45] Thus, the incorporation of a relatively small amount of Ag into the Cu surface will result in compressive strain in the majority of Cu surface atoms.

Strain has been identified both theoretically and experimentally as a means of modifying the electrocatalytic activity of transition metals.[46−48] This electrocatalytic activity modification arises due to changes in the valence band structure of the strained metal, with compressive strain inducing a shift of the valence band density of states to higher binding energies.[49] Since the interaction of the valence orbitals of a transition metal with the electronic orbitals of the adsorbate is what determines

DOI: 10.1021/jacs.7b08607
J. Am. Chem. Soc. 2017, 139, 15848−15857

the adsorption energy, these strain-induced electronic modifications are accompanied by a concomitant shift in the adsorption energy of reactive chemical species.[46,50,51] The magnitude of these adsorption energy shifts scale with the magnitude of the lateral surface strain, with the adsorption energy of O being roughly 5 times more sensitive to strain effects than CO.[52,53] As the valence band density of states shifts to higher binding energies there is generally less interaction with the electronic orbitals of adsorbates, resulting in the population of the antibonding orbital and a weak adsorption energy.[54,55]

To provide evidence for the presence of electronic modifications in the CuAg bimetallic electrodes and surface alloys consistent with compressive strain, the valence band density of states of the bimetallic electrodes were measured and compared to what would be expected if they behaved as a linear combination of Cu and Ag (see Supporting Information, SI-22). As shown in Figure 7, the valence band density of states of

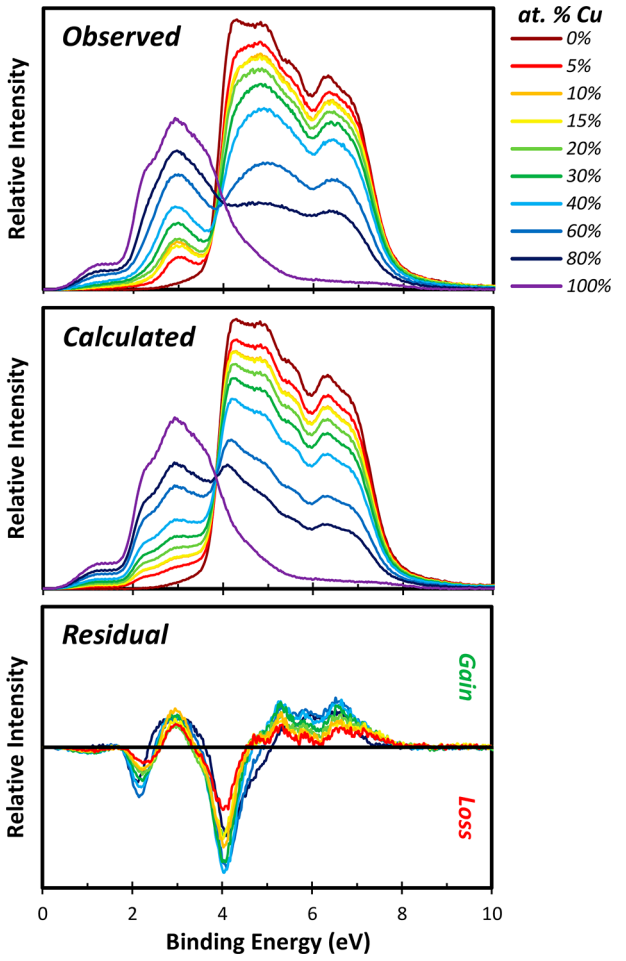

Figure 7. Valence band spectra of the CuAg bimetallic electrodes.

the CuAg bimetallic electrodes behave largely as a linear combination of Cu and Ag. However, subtle differences in the observed valence band at binding energies below 3.5 eV suggest that the valence band density of states of the Cu phase in the bimetallic electrodes has shifted to higher binding energies. Furthermore, the magnitude of the shift is nearly independent of the bulk composition of the bimetallic electrodes, consistent with the notion that the surface of the Cu phase in the bimetallic electrodes consists of a CuAg surface alloy with a saturated Ag content. It is important to note that such valence band modifications can also arise due to ligand effects, wherein a formal electron transfer between the constituent metals occurs.[55] However, the driving force for such an electron transfer is either a difference in the electronegativity of the constituent metals or a difference in the fraction of their valence bands that are populated by electrons.[56−59] Since Cu and Ag have equally filled valence bands, and possess nearly identical electronegativities, there is no driving force for an electron transfer between Cu and Ag. This hypothesis was confirmed by the lack of a shift in the binding energies of the Cu 2p or Ag 3d core levels in the bimetallic electrodes, which would be expected if an electron transfer between the constituent metals occurred (see Supporting Information, SI-23).

As previously stated, the binding energy of O is roughly 5 times more sensitive to strain effects than CO.[53] Conveniently, the oxophilicity of transition metals is highly correlated with their standard reduction potentials (see Supporting Information, SI-24). Thus, cyclic voltammetry can be utilized to determine if the compressive strain induced by the incorporation of Ag atoms into the Cu surface results in an observable reduction of the oxophilicity of Cu (see SI-25). As shown in Figure 8, the Cu^{2+}/Cu^{+} reduction wave is shifted to more

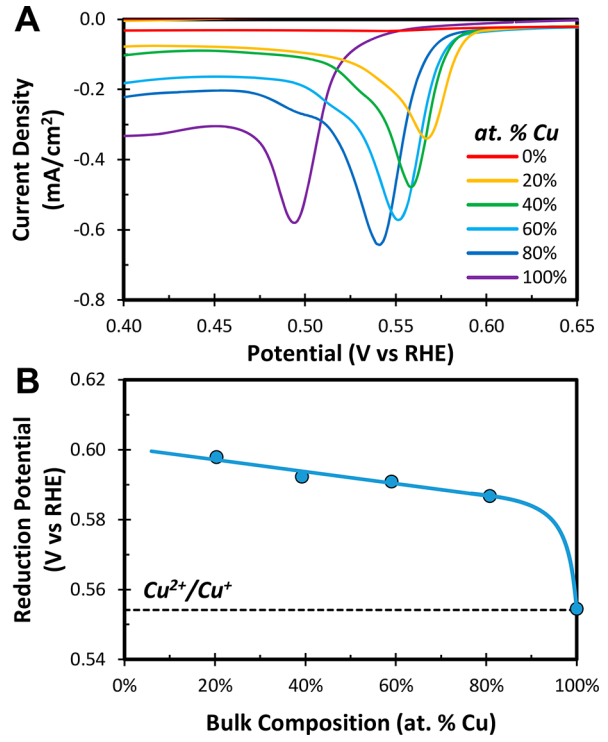

Figure 8. (A) Cu^{2+}/Cu^{+} reduction waves observed during cyclic voltammetry over the CuAg bimetallic electrodes. (B) Onset potential of the Cu^{2+}/Cu^{+} reduction wave observed during cyclic voltammetry over the CuAg bimetallic electrodes.

anodic potentials over the bimetallic electrodes compared to pure Cu, consistent with the notion that the Cu surface is compressively strained by surface alloying with Ag.

Impact of Compressive Strain on the Reaction Kinetics and Product Selectivity. The activity descriptor for HER over transition metals has been shown theoretically to be the H adsorption energy.[60−62] Since monometallic Cu has a suboptimal H adsorption energy, the adsorption of H is the

DOI: 10.1021/jacs.7b08607
J. Am. Chem. Soc. 2017, 139, 15848−15857

Scheme 1. Proposed Reaction Mechanisms Leading to C_1 and C_2 Products[a]

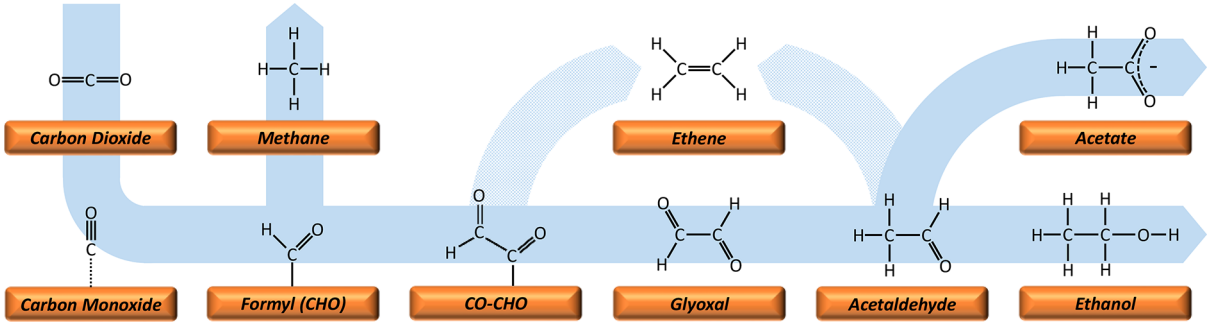

[a]Light blue arrows denote potential pathways to ethene.

rate-determining step of HER over Cu.[60] Thus, weakening the H adsorption energy by compressive strain should reduce the HER activity of Cu further by reducing the fraction of the surface covered by adsorbed hydrogen atoms. Conversely, the activity descriptor of CO_2RR has been proposed to be the CO adsorption energy since the reduction of CO is the rate-determining step in the reduction of CO_2 to hydrocarbons and alcohols over Cu.[7−10,63] Thus, one would expect the rates of CO_2RR over Cu to be influenced by compressive strain, in contrast to what is observed in the present work. To reconcile this apparent inconsistency one must consider the differences in the site of adsorption for H and CO. While it is difficult to observe adsorbed H spectroscopically, theory has found that H adsorbs in the hollow site on both the Cu(111) and Cu(100) surfaces.[64] Conversely, infrared absorption studies have found that CO adsorbs on the ontop site on Cu surfaces under electrochemical conditions.[65−67] Thus, H and CO adsorb on different surface sites, the electronic properties of which are modified by different magnitudes by surface strain. A recent theoretical study of Cu-based surface alloys found that H adsorbed in the hollow site was more significantly destabilized by compressive strain than CO adsorbed on the ontop site.[68] Thus, compressive strain results in a reduction of the adsorption energy of H relative to CO, leading to an enhanced selectivity for the production of products derived from CO by selective suppression of HER.

Theoretical studies have found that the lowest energy pathway to C−C coupling at potentials cathodic of −1 V vs RHE over Cu(100) involves the reaction of CO with CHO to form CO−CHO.[69] This intermediate could be reduced to glyoxal, the simplest C_2 product produced by CO_2RR over Cu.[12] Furthermore, it has been shown that glyoxal reduction produces acetaldehyde over pure Cu and that at more cathodic potentials acetaldehyde can be reduced further to yield ethanol.[8,70,71] The reduction of glyoxal is relatively facile in comparison to CO_2RR unlike the reduction of acetaldehyde, which requires a slightly lower overpotential than the reduction of CO.[70] This observation suggests that acetaldehyde has a relatively weak binding energy to the Cu surface compared to other carbonyl-containing intermediate reaction products. Thus, the enhanced production of acetaldehyde may be a result of the reduced oxophilicity of the compressively strained Cu, which presumably reduces the acetaldehyde adsorption energy to the extent that it desorbs from the Cu surface as it is produced. Once desorbed, acetaldehyde may then be susceptible to "Cannizzaro-type" disproportionation in the relatively alkaline conditions found within the hydrodynamic boundary layer at the cathode surface, producing ethanol and acetate.[72] This would explain the correlation between the generation rates of acetate and acetaldehyde observed here and reported elsewhere.[73] Interestingly, the molar ratio of acetate to acetaldehyde was observed to be constant in all experiments performed despite nearly an order of magnitude variation in their absolute generation rates (see Supporting Information, SI-26). The observed acetate to acetaldehyde molar ratio is equivalent to the equilibrium constant of acetaldehyde hydration in water, suggesting that the formation of 1,1-ethanediol by hydration of acetaldehyde may initiate the "Cannizzaro-type" disproportionation.

It is difficult to explain why the enhanced production rate of carbonyl-containing products comes at the expense of ethene because little is known about the mechanism leading to ethene formation from CO. One potential explanation is that acetaldehyde intermediates are present on the electrode surface as vinyl alcohol, the keto form of acetaldehyde, and that this species can be reduced to ethene.[12] An alternative mechanism is that the ethene pathway diverges from the ethanol pathway before the formation of glyoxal. These potential routes are summarized in Scheme 1. Interestingly, a recent theoretical study has concluded that surface adsorbed water plays a critical role in determining the hydrocarbon selectivity observed over Cu by initiating C−O bond scission.[74] Thus, the enhanced formation of carbonyl-containing products at the expense of ethene may be a result of the suppression of HER, which also reduces the rate of C−O bond scission by reducing the surface coverage of HER intermediates. This hypothesis is supported by the inverse correlation between the oxygenate selectivity, defined as the fraction of the current going toward the production of products derived from CO that are oxygenates, and the HER activity observed over the Cu(100)+Ag surface alloys, as shown in Figure 9. Thus, the addition of Ag into the Cu surface enhances the oxygenate selectivity observed during CO_2RR by selectively titrating HER active surface sites.

■ CONCLUSIONS

As-prepared CuAg bimetallic electrodes consist of Cu and Ag crystallites with a surface composition equivalent to that of the bulk. However, during CO_2RR the Ag-rich bimetallic electrodes undergo Cu surface enrichment due to CO adsorbate-induced segregation of the Cu initially dissolved in the Ag phase. The distribution of products produced over stable CuAg bimetallic electrodes indicate that CO is primarily produced on the surface of the Ag domains, whereas CO reduction occurs exclusively on the surface of the Cu domains. However, the distribution of products observed over the Cu domains is

DOI: 10.1021/jacs.7b08607
J. Am. Chem. Soc. 2017, 139, 15848−15857

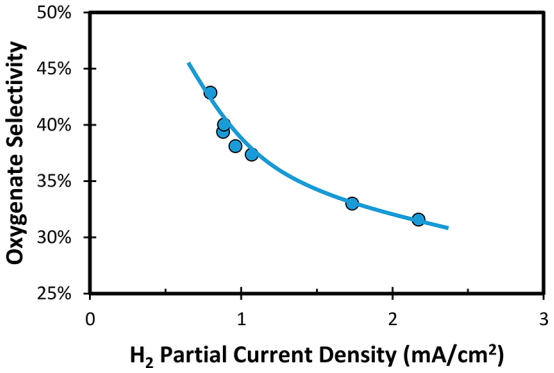

Figure 9. Oxygenate selectivity as a function of the HER activity of the Cu(100)+Ag surface alloys measured at an applied potential of −1 V vs RHE.

altered compared to pure Cu, with H_2 production being suppressed by ∼75%. While the suppression of HER does not inhibit the ability of the Cu domains to produce products derived from CO, the distribution of products shifts to favor carbonyl-containing products at the expense of hydrocarbons. This activity modification was found to be independent of the near-surface composition of the bimetallic electrodes, suggesting that the Cu phase is equally modified by a small amount of Ag in all cases. The mechanism of surface promotion is compressive strain induced by the formation of a Cu+Ag surface alloy, which induces a shift in the valence band density of states of Cu to deeper levels. This interpretation is strongly supported by observations over Cu+Ag surface alloys prepared by Galvanic exchange of Ag into Cu(100) thin films, which display a shift in product selectivity by the addition of <3 at.% Ag into the near-surface region that is in good agreement with those observed over the Cu phase in the bimetallic electrodes.

Thus, the incorporation of Ag atoms into the Cu surface results in compressive strain in the neighboring Cu atoms, which induces an observable shift in the valence band density of states of Cu to deeper levels. This electronic structure modification reduces the binding energies of H and O relative to CO, leading to an enhanced selectivity for the production of products derived from CO due to the selective suppression of HER. These strain effects also result in an enhanced selectivity to multi-carbon carbonyl-containing products at the expense of ethene due to the reduced coverage of adsorbed H and the reduced oxophilicity of the compressively strained Cu. These insights provide a rational means for modifying the activity of CO_2RR electrocatalysts to favor the formation of oxygenated products.

■ ASSOCIATED CONTENT

Supporting Information

The Supporting Information is available free of charge on the ACS Publications website at DOI: 10.1021/jacs.7b08607.

Experiments and analyses (PDF)

■ AUTHOR INFORMATION

Corresponding Author

*alexbell@berkeley.edu

ORCID

Christopher Hahn: 0000-0002-2772-6341

Thomas F. Jaramillo: 0000-0001-9900-0622

Alexis T. Bell: 0000-0002-5738-4645

Notes

The authors declare no competing financial interest.

■ ACKNOWLEDGMENTS

This material is based upon work performed by the Joint Center for Artificial Photosynthesis, a DOE Energy Innovation Hub, supported through the Office of Science of the U.S. Department of Energy under Award Number DE-SC0004993. E.L.C. was supported by the National Science Foundation. The authors would also like to acknowledge Dr. Jason Cooper for assistance with the XPS and ISS measurements, Dr. Youngkook Kwon for configuring the HPLC, Dr. Peter Lobacarro for improving the electrochemical cell design, James Wu for preparing the bimetallic foils, and Eric Granlund for fabricating the electrochemical cell.

■ REFERENCES

(1) Jitaru, M.; Lowy, D. A.; Toma, M.; Toma, B. C.; Oniciu, L. *J. Appl. Electrochem.* **1997**, *27*, 875−889.

(2) Gattrell, M.; Gupta, N.; Co, a. *J. Electroanal. Chem.* **2006**, *594*, 1−19.

(3) Hori, Y. In *Modern Aspects of Electrochemistry*; Vayenas, C. G., White, R. E., Gamboa-Aldeco, M. E., Eds.; Springer: New York, 2008; pp 89−189.

(4) Hori, Y.; Kikuchi, K.; Suzuki, S. *Chem. Lett.* **1985**, *14*, 1695−1698.

(5) Noda, H.; Ikeda, S.; Oda, Y.; Imai, K.; Maeda, M.; Ito, K. *Bull. Chem. Soc. Jpn.* **1990**, *63*, 2459−2462.

(6) Hori, Y.; Murata, A.; Takahashi, R.; Suzuki, S. *Chem. Lett.* **1987**, *16*, 1665−1668.

(7) Hori, Y.; Murata, A.; Takahashi, R. *J. Chem. Soc., Faraday Trans. 1* **1989**, *85*, 2309−2326.

(8) Hori, Y.; Takahashi, R.; Yoshinami, Y.; Murata, A. *J. Phys. Chem. B* **1997**, *101*, 7075−7081.

(9) Peterson, A. A.; Abild-Pedersen, F.; Studt, F.; Rossmeisl, J.; Nørskov, J. K. *Energy Environ. Sci.* **2010**, *3*, 1311−1315.

(10) Peterson, A. A.; Nørskov, J. K. *J. Phys. Chem. Lett.* **2012**, *3*, 251−258.

(11) Nie, X.; Esopi, M. R.; Janik, M. J.; Asthagiri, A. *Angew. Chem., Int. Ed.* **2013**, *52*, 2459−2462.

(12) Kuhl, K. P.; Cave, E. R.; Abram, D. N.; Jaramillo, T. F. *Energy Environ. Sci.* **2012**, *5*, 7050−7059.

(13) Noda, H.; Ikeda, S.; Oda, Y.; Ito, K. *Chem. Lett.* **1989**, *18*, 289−292.

(14) Li, C. W.; Kanan, M. W. *J. Am. Chem. Soc.* **2012**, *134*, 7231−7234.

(15) Tang, W.; Peterson, A. A.; Varela, A. S.; Jovanov, Z. P.; Bech, L.; Durand, W. J.; Dahl, S.; Nørskov, J. K.; Chorkendorff, I. *Phys. Chem. Chem. Phys.* **2012**, *14*, 76−81.

(16) Manthiram, K.; Beberwyck, B. J.; Alivisatos, A. P. *J. Am. Chem. Soc.* **2014**, *136*, 13319−13325.

(17) Roberts, F. S.; Kuhl, K. P.; Nilsson, A. *Angew. Chem., Int. Ed.* **2015**, *54*, 5179−5182.

(18) Feng, X.; Jiang, K.; Fan, S.; Kanan, M. W. *ACS Cent. Sci.* **2016**, *2*, 169−174.

(19) Murata, A.; Hori, Y. *Bull. Chem. Soc. Jpn.* **1991**, *64*, 123−127.

(20) Kyriacou, G. Z.; Anagnostopoulos, A. K. *J. Appl. Electrochem.* **1993**, *23*, 483−486.

(21) Singh, M. R.; Kwon, Y.; Lum, Y.; Ager, J. W.; Bell, A. T. *J. Am. Chem. Soc.* **2016**, *138*, 13006−13012.

(22) Hori, Y.; Murata, A.; Takahashi, R.; Suzuki, S. *J. Chem. Soc., Chem. Commun.* **1988**, *1*, 17−19.

(23) Kas, R.; Kortlever, R.; Yılmaz, H.; Koper, M. T. M.; Mul, G. *ChemElectroChem* **2015**, *2*, 354−358.

(24) Varela, A. S.; Kroschel, M.; Reier, T.; Strasser, P. *Catal. Today* **2016**, *260*, 8−13.

DOI: 10.1021/jacs.7b08607
J. Am. Chem. Soc. 2017, 139, 15848−15857

(25) Hansen, H. A.; Shi, C.; Lausche, A.; Peterson, A.; Nørskov, J. K. *Phys. Chem. Chem. Phys.* **2016**, *18*, 9194−9201.
(26) Hahn, C.; Abram, D. N.; Hansen, H. A.; Hatsukade, T.; Jackson, A.; Johnson, N. C.; Hellstern, T. R.; Kuhl, K. P.; Cave, E. R.; Feaster, J. T.; Jaramillo, T. F. *J. Mater. Chem. A* **2015**, *3*, 20185−20194.
(27) Ren, D.; Ang, B. S.-H.; Yeo, B. S. *ACS Catal.* **2016**, *6*, 8239−8247.
(28) Torelli, D. A.; Francis, S. A.; Crompton, J. C.; Javier, A.; Thompson, J. R.; Brunschwig, B. S.; Soriaga, M. P.; Lewis, N. S. *ACS Catal.* **2016**, *6*, 2100−2104.
(29) Ma, S.; Sadakiyo, M.; Heima, M.; Luo, R.; Haasch, R. T.; Gold, J. I.; Yamauchi, M.; Kenis, P. J. A. *J. Am. Chem. Soc.* **2017**, *139*, 47−50.
(30) Hori, Y.; Murata, A.; Yoshinami, Y. *J. Chem. Soc., Faraday Trans.* **1991**, *87*, 125−128.
(31) Hori, Y.; Koga, O.; Yamazaki, H.; Matsuo, T. *Electrochim. Acta* **1995**, *40*, 2617−2622.
(32) Zhang, Y.-J.; Sethuraman, V.; Michalsky, R.; Peterson, A. *ACS Catal.* **2014**, *4*, 3742−3748.
(33) Hori, Y.; Murata, A.; Ito, S.-Y.; et al. *Chem. Lett.* **1989**, *18*, 1567−1570.
(34) Monzo, F. J.; Malewski, Y.; Kortlever, R.; Vidal-Iglesias, F. J.; Solla-Gullon, J.; Koper, M. T. M.; Rodriguez, P. *J. Mater. Chem. A* **2015**, *3*, 23690−23698.
(35) Wuttig, A.; Liu, C.; Peng, Q.; Yaguchi, M.; Hendon, C. H.; Motobayashi, K.; Ye, S.; Osawa, M.; Surendranath, Y. *ACS Cent. Sci.* **2016**, *2*, 522−528.
(36) Hatsukade, T.; Kuhl, K. P.; Cave, E. R.; Abram, D. N.; Jaramillo, T. F. *Phys. Chem. Chem. Phys.* **2014**, *16*, 13814−13819.
(37) Subramanian, P. R.; Perepezko, J. H. *J. Phase Equilib.* **1993**, *14*, 62−75.
(38) Krastev, E. T.; Voice, L. D.; Tobin, R. G. *J. Appl. Phys.* **1996**, *79*, 6865−6871.
(39) Jiang, H.; Klemmer, T. J.; Barnard, J. A.; Payzant, E. A. *J. Vac. Sci. Technol., A* **1998**, *16*, 3376−3383.
(40) Lobaccaro, P.; Singh, M. R.; Clark, E. L.; Kwon, Y.; Bell, A. T.; Ager, J. W. *Phys. Chem. Chem. Phys.* **2016**, *18*, 26777−26785.
(41) Dunwell, M.; Lu, Q.; Heyes, J. M.; Rosen, J.; Chen, J. G.; Yan, Y.; Jiao, F.; Xu, B. *J. Am. Chem. Soc.* **2017**, *139*, 3774−3783.
(42) Wuttig, A.; Surendranath, Y. *ACS Catal.* **2015**, *5*, 4479−4484.
(43) Hahn, C.; Hatsukade, T.; Kim, Y.; Vailionis, A.; Baricuatro, J. H.; Higgins, D. C.; et al. *Proc. Natl. Acad. Sci. U. S. A.* **2017**, *114*, 5918−5923.
(44) Sprunger, P. T.; Lægsgaard, E.; Besenbacher, F. *Phys. Rev. B: Condens. Matter Mater. Phys.* **1996**, *54*, 8163−8171.
(45) Christensen, A.; Ruban, A.; Stoltze, P.; Jacobsen, K.; Skriver, H.; Nørskov, J. K.; Besenbacher, F. *Phys. Rev. B: Condens. Matter Mater. Phys.* **1997**, *56*, 5822−5834.
(46) Hammer, B.; Morikawa, Y.; Nørskov, J. *Phys. Rev. Lett.* **1996**, *76*, 2141−2144.
(47) Kibler, L. A.; El-Aziz, A. M.; Hoyer, R.; Kolb, D. M. *Angew. Chem., Int. Ed.* **2005**, *44*, 2080−2084.
(48) Sandberg, R. B.; Montoya, J. H.; Chan, K.; Nørskov, J. K. *Surf. Sci.* **2016**, *654*, 56−62.
(49) Ruban, A.; Hammer, B.; Stoltze, P.; Skriver, H. L.; Nørskov, J. K. *J. Mol. Catal. A: Chem.* **1997**, *115*, 421−429.
(50) Nilsson, A.; Pettersson, L. G. M.; Hammer, B.; Bligaard, T.; Christensen, C. H.; Nørskov, J. K. *Catal. Lett.* **2005**, *100*, 111−114.
(51) Xin, H.; Vojvodic, A.; Voss, J.; Nørskov, J. K.; Abild-Pedersen, F. *Phys. Rev. B: Condens. Matter Mater. Phys.* **2014**, *89*, 115114.
(52) Kampshoff, E.; Hahn, E.; Kern, K. *Phys. Rev. Lett.* **1994**, *73*, 704−707.
(53) Mavrikakis, M.; Hammer, B.; Nørskov, J. *Phys. Rev. Lett.* **1998**, *81*, 2819−2822.
(54) Hammer, B.; Nørskov, J. K. *Surf. Sci.* **1995**, *343*, 211−220.
(55) Bligaard, T.; Nørskov, J. K. *Electrochim. Acta* **2007**, *52*, 5512−5516.
(56) Rodriguez, J. A.; Campbell, R. A.; Goodman, D. W. *J. Phys. Chem.* **1990**, *94*, 6936−6939.
(57) Rodriguez, J. A.; Campbell, R. A.; Goodman, D. W. *J. Phys. Chem.* **1991**, *95*, 5716−5719.
(58) Rodriguez, J. A.; Goodman, D. W. *Science* **1992**, *257*, 897−903.
(59) Rodriguez, J. A.; Campbell, R. A.; Goodman, D. W. *Surf. Sci.* **1994**, *307*−*309*, 377−383.
(60) Nørskov, J. K.; Bligaard, T.; Logadottir, A.; Kitchin, J. R.; Chen, J. G.; Pandelov, S.; Stimming, U. *J. Electrochem. Soc.* **2005**, *152*, J23−J26.
(61) Sheng, W.; Zhuang, Z.; Gao, M.; Zheng, J.; Chen, J. G.; Yan, Y. *Nat. Commun.* **2015**, *6*, 5848.
(62) Zheng, J.; Sheng, W.; Zhuang, Z.; Xu, B.; Yan, Y. *Sci. Adv.* **2016**, *2*, e1501602.
(63) Kuhl, K. P.; Hatsukade, T.; Cave, E. R.; Abram, D. N.; Kibsgaard, J.; Jaramillo, T. F. *J. Am. Chem. Soc.* **2014**, *136*, 14107−14113.
(64) Kratzer, P.; Hammer, B.; Nørskov, J. *Surf. Sci.* **1996**, *359*, 45−53.
(65) Miyake, H.; Osawa, M. *Chem. Lett.* **2004**, *33*, 278−279.
(66) Wang, H. F.; Yan, Y. G.; Huo, S. J.; Cai, W. B.; Xu, Q. J.; Osawa, M. *Electrochim. Acta* **2007**, *52*, 5950−5957.
(67) Heyes, J.; Dunwell, M.; Xu, B. *J. Phys. Chem. C* **2016**, *120*, 17334−17341.
(68) Sarfraz, S.; Garcia-Esparza, A. T.; Jedidi, A.; Cavallo, L.; Takanabe, K. *ACS Catal.* **2016**, *6*, 2842−2851.
(69) Goodpaster, J. D.; Bell, A. T.; Head-Gordon, M. *J. Phys. Chem. Lett.* **2016**, *7*, 1471−1477.
(70) Schouten, K. J. P.; Kwon, Y.; van der Ham, C. J. M.; Qin, Z.; Koper, M. T. M. *Chem. Sci.* **2011**, *2*, 1902−1909.
(71) Bertheussen, E.; Verdaguer-Casadevall, A.; Ravasio, D.; Montoya, J. H.; Trimarco, D. B.; Roy, C.; Meier, S.; Wendland, J.; Nørskov, J. K.; Stephens, I. E. L.; Chorkendorff, I. *Angew. Chem., Int. Ed.* **2016**, *55*, 1450−1454.
(72) Birdja, Y. Y.; Koper, M. T. M. *J. Am. Chem. Soc.* **2017**, *139*, 2030−2034.
(73) Hori, Y.; Takahashi, I.; Koga, O.; Hoshi, N. *J. Mol. Catal. A: Chem.* **2003**, *199*, 39−47.
(74) Xiao, H.; Cheng, T.; Goddard, W. A. *J. Am. Chem. Soc.* **2017**, *139*, 130−136.

DOI: 10.1021/jacs.7b08607
J. Am. Chem. Soc. 2017, 139, 15848−15857